

# Extinction and coexistence in a binary mixture of proliferating motile disks

Alejandro Almodóvar,<sup>\*</sup> Tobias Galla,<sup>†</sup> and Cristóbal López<sup>‡</sup>  
*IFISC, Instituto de Física Interdisciplinar y Sistemas Complejos (CSIC-UIB),  
Campus Universitat de les Illes Balears, E-07122 Palma de Mallorca, Spain*

A binary mixture of two-different-sizes proliferating motile disks is studied. As growth is space-limited, we focus on the conditions such that there is coexistence of both large and small disks, or dominance of the larger disks. The study involves systematically varying some system parameters, such as diffusivities, growth rates, and self-propulsion velocities. In particular, we demonstrate that diffusing faster confers a competitive advantage, so that larger disks can in the long time coexist or even dominate to the smaller ones. In the case of self-propelled disks a coexistence regime is induced by the activity where the two types of disks show the same spatial distribution: both phase separated or both homogeneously distributed in the whole system.

## I. INTRODUCTION

Motivated by the collective dynamics in biological phenomena such as wound healing [1–3], tissue formation [4], the expansion of tumours [5], or the dynamics of bacterial populations [6], there is growing interest in the study of proliferating motile matter [7, 8]. These are often modelled as interacting particle systems [3, 5, 9, 10], and the number of particles may not be constant in time due to processes such as birth and death. Coupled with individual movement one can expect new emergent properties. For example, we recently introduced a simple model of *proliferating* motile finite-size particles. Specifically, in [11] we studied both systems of passive disks (where motility has its origins in a thermal bath) and self-propelled disks [12–16] subject to reproduction and death. We analysed different emerging structural phases [liquid, hexatic, solid and motility-induced phase separation (MIPS)] [16–22]. These phases result as a consequence of the disks filling the available space, and the phase that is realised depends on parameters such as the birth and death rates, and the motility.

In [11] we focussed on a two-dimensional collection of disks (we will refer to these also as particles), which were all taken to be identical, in particular, they have the same size. This is not realistic in many biological applications. In the current work we analyse the influence on some properties of the system when relaxing this condition, and consider a binary mixture of disks of two different sizes [23, 24]. In the standard equilibrium system of hard disks (without birth-death events or activity) the two-sizes binary mixture is known to have important effects leading for example to the disappearance of the hexatic phase even for very low concentration of small disks [25]. Thus we expect new behavior in a non-equilibrium model of a binary mixture with birth and death dynamics.

We start with a similar concentration for both types (or species) of disks, initially randomly distributed in a two-dimensional space. As the system evolves, particles move,

die and reproduce, eventually filling up space. Due to the death processes it is possible for one species to go extinct. In reproduction events a new particle is created in the system, with the same size as the parent, and placed close to it if there is enough room.

As in many real-world systems, reproduction in our model is limited by the available space [26–28]. Under identical conditions, the smaller disks have a higher a-priori chance to reproduce, and therefore to persist in the long-run. Even though the availability of space puts the larger particles at a disadvantage [29, 30], we find that, depending on motility and demography, coexistence of both species can occur. In some other cases we find that the larger particles can dominate the system, i.e. their number is much larger than that of the smaller particles, typically more than 90% of the total particle number.

The main questions we address are what type of disk dominates the system in the long-run, under what conditions both types co-exist, and, in the important case of activity-induced phase separation, what the resulting spatial structure is. We are interested in the influence of the birth and death rates and the motilities of the particles on the outcome. In particular, we ask which population survives when the two species compete (due to reproduction limited by size) with different diffusivities [31, 32], and we show results that support the prevalence of the fast diffusing type of particle. Our overall aim is to characterise the system behaviour for different choices of the model parameters.

In the case of active motion [33–35] we also study what the conditions are under which the spatial distribution of the particles presents coexisting dilute and dense phases, i.e., the MIPS regime. This is for example motivated by studies hypothesizing that phase heterogeneity due to MIPS can trigger a transition from swarming behaviour to biofilm formation in some type of bacteria [36]. We analyse the role of this heterogeneity for the dominance dynamics of the binary mixture.

Throughout our analysis, we will mostly concentrate on systems in which the diameter of one type of disk is 20% larger than the other, but we will also discuss other size ratios [37–40].

The remainder of the paper is organised as follows. In

<sup>\*</sup> [almodovar@ifisc.uib-csic.es](mailto:almodovar@ifisc.uib-csic.es)

<sup>†</sup> [tobias.galla@ifisc.uib-csic.es](mailto:tobias.galla@ifisc.uib-csic.es)

<sup>‡</sup> [clopez@ifisc.uib-csic.es](mailto:clopez@ifisc.uib-csic.es)

Sec. II, we present the model of mobile disks undergoing birth and death dynamics. The main outcomes are presented in Sec. III. A summary and discussion of the findings is contained in Sec. IV.

## II. MODEL AND NUMERICAL ALGORITHM

The model is similar to that in [11] but with particles of two different sizes. We consider a two-dimensional system of  $N(t) = N_L(t) + N_S(t)$  interacting disks with diameters  $\sigma_S$  and  $\sigma_L$  such that  $\sigma_S < \sigma_L$  ( $S$  and  $L$  stands for ‘small’ and ‘large’, respectively). The particle numbers can change in time, due to birth and death events, as explained below. We consider the overdamped limit and take the friction coefficient to be equal to unity for both species. The motion of disks is then as follows,

$$\dot{\mathbf{r}}_i = \mathbf{F}_i + \mathbf{F}_i^{act} + \sqrt{2D_i}\zeta_i(t), \quad i = 1, \dots, N(t). \quad (1)$$

If disk  $i$  is of the small type then  $D_i = D_S$ , and if it is of the large type then  $D_i = D_L$ . The variables  $\{\zeta_i\}$  are independent Gaussian noise vectors satisfying  $\langle \zeta_i \rangle = 0$ ,  $\langle \zeta_{i,a}(t)\zeta_{j,b}(t') \rangle = \delta_{ij}\delta_{ab}\delta(t-t')$  ( $a$  and  $b$  are the entries of the two-component vectors  $\zeta_i$  and  $\zeta_j$ ). No Einstein relation is assumed, and  $D_L$  and  $D_S$  are taken as parameters of the model. The finite size of the disks is simulated using a truncated Lennard-Jones potential so that the force on particle  $i$  resulting from the interaction with the rest of particles is  $\mathbf{F}_i = -\nabla_i \sum_{i \neq j} U(|\mathbf{r}_i - \mathbf{r}_j|)$ , where the potential is given by (with  $r = |\mathbf{r}_i - \mathbf{r}_j|$ )

$$U(r) = 4\varepsilon \left[ \left( \frac{\sigma_{ij}}{r} \right)^{12} - \left( \frac{\sigma_{ij}}{r} \right)^6 \right] + \varepsilon, \quad (2)$$

if  $r < 2^{1/6}\sigma_{ij}$ , and  $U(r) = 0$  if  $r > 2^{1/6}\sigma_{ij}$ . The quantity  $\sigma_{ij} > 0$  is defined from the Lorentz-Berthelot rule as  $\sigma_{ij} = (\sigma_i + \sigma_j)/2$ , where  $\sigma_i$  and  $\sigma_j$  are the diameters of disks  $i$  and  $j$ , respectively. Thus,  $\sigma_{ij}$  reflects the effective distance between the two disks. The parameter  $\varepsilon$  is an energy scale [41, 42].

In some of our numerical experiments particles are self-propelled. We model this using active forces

$$\mathbf{F}_i^{act} = v_i \mathbf{n}[\theta_i(t)] \quad (3)$$

of constant modulus  $v_i = \{v_L, v_S\}$  (typically called activity or velocity) and with a direction given by the unit vector  $\mathbf{n}(\theta_i) = (\cos \theta_i, \sin \theta_i)$ . The angle  $\theta_i$  for disk  $i$  performs diffusive motion,  $\dot{\theta}_i(t) = \sqrt{2D_r}\eta_i(t)$ . The term  $\eta_i$  represents a zero-mean Gaussian noise with  $\langle \eta_i(t)\eta_j(t') \rangle = \delta_{ij}\delta(t-t')$ .

In addition to movement and interaction, disks may randomly self-replicate or die, so that the number of disks of each type,  $N_L(t)$  and  $N_S(t)$ , can change with time. These events occur as follows (see [11] for further details of the algorithm):

1. Death occurs as a Poisson process. Each existing particle dies with per capita rate  $\delta$ . Particles that die are removed from the system.

2. Potential births are triggered with per capita rate  $\beta_L$  for large disks, and  $\beta_S$  for small disks. The diameter of the potential offspring is identical to that of the parent. The birth event only occurs if there is sufficient space around the parent particle to place the offspring without overlapping with any other disk. If there is no space, no birth event occurs. This means that not all potential reproduction events complete.

We always assume that the growth rates  $\beta_S$  and  $\beta_L$  are larger than the death rate (the latter is taken to be equal for all the disks), i.e.  $\beta_L, \beta_S > \delta$ . At long times the system reaches a stationary state. The numbers of disks of each type in this state are such that the mean effective birth rate for each species is equal to the death rate.

In the next sections we study this steady state while varying one or two model parameters at a time (e.g., the diffusivity of both types of particles, the growth rates or activity). Our main objective is to study what type of disk dominates, and under what conditions there is coexistence.

## III. RESULTS

We consider a two-dimensional box of length  $L_s = 150$  with periodic boundary conditions,  $\delta = 0.01$ , and for the most part  $\sigma_S = 1.0$  and  $\sigma_L = 1.2$ , supplemented by some discussion of other choices of the diameters. For simplicity, we set  $\varepsilon = 1.0$  and  $D_r = 1.0$ . Simulation results are independent of  $\delta$  whose role is mostly to set the time scale needed to reach the steady state [11]. We start with 250 particles of each size, together occupying around 8% of the total area. We compute the packing fraction for particles of type. We write these as  $\phi_\alpha(t) = N_\alpha(t)\pi(\sigma_\alpha/2)^2/L_s^2$  for  $\alpha \in \{L, S\}$ , where  $N_\alpha(t)$  is the number of particles of type  $\alpha$  at time  $t$ .

We study passive particles in Sec. III A. Systems of active particles are discussed in Sec. III B.

### A. Passive particles

We set  $\mathbf{F}_i^{act} = 0$ , and study the effects of the parameters of the demographic dynamics, and of the diffusivities separately.

#### 1. Effects of the birth and death rates

We fix the diffusivities to low values (i.e. the time scale of a disk to move a distance of the order of several diameters is large compared to its typical lifetime)  $D_L = D_S = 0.001$ , to focus on the effects of the birth and death dynamics. Since reproduction is limited by the available space, we naively expect only the smaller disks to be present in the long-run

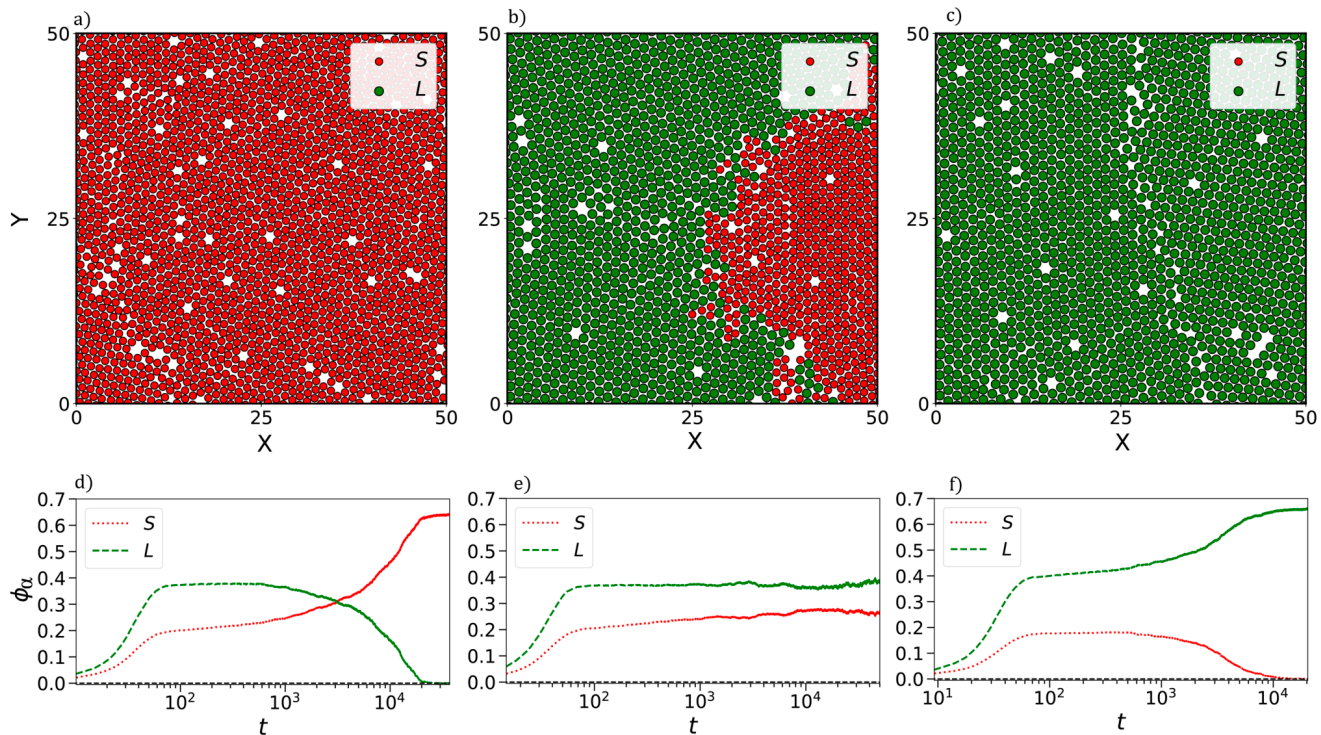


Figure 1. Panels in the first row (a-c) show snapshots of the spatial distribution of passive disks in space at long times (only a part of the full size  $L_s = 150$  is shown). Panels in the second row (d-f) correspond to the temporal evolution of the packing fraction starting with a random configuration of 250 disks of each type. In each column, we have used different values of  $\beta_L$ , at fixed  $\beta_S = 0.1$ , and  $\beta_L = 0.114, 0.118, 0.13$  from left to right. The remaining parameters are  $\delta = 0.01$ ,  $D = 0.001$ ,  $\sigma_L/\sigma_S = 1.2$ .

when the raw birth rates of both types are similar. However, the outcome may be different if the birth rate for the larger particles is much larger than that of the smaller type. This is indeed what we observe in the numerical experiments shown in Fig. 1.

In the upper row of Fig. 1 we plot snapshots of the spatial distribution of disks in the stationary state. Smaller particles shown in red, larger ones in green. The growth rate of the small particles is lower than that of the larger particles in all three panels, but the ratio  $\beta_L/\beta_S$  increases from left to right. In panel a) we observe the extinction of the larger particles, in panel b) we find balanced co-existence throughout the simulation, and in panel c) the ratio  $\beta_L/\beta_S$  is sufficiently large for the larger disks to fully dominate (the smaller particles go extinct). In the lower panels of Fig. 1 we plot the corresponding time evolution of the packing fractions (the snapshots in the upper panels are taken at the final time of the lower ones). These time series confirm the extinction of the larger type of particle [panel d)], co-existence [panel e)] and the extinction of the smaller type [panel f)], respectively. In all three situations, and regardless of the final fate of the larger particles, there is initially a faster increase of the packing of the larger particles. This is because  $\beta_L > \beta_S$  in all panels in Fig. 1

In Fig. 2a) we plot the phase diagram in the plane of birth rates for the two species (each divided by the death rate

$\delta = 0.01$ ). The colored heatmap indicates the normalised packing fraction  $\phi_S/(\phi_S + \phi_L)$  of the smaller disks. In Fig. 2b) we show the respective packing fractions of both types when varying  $\beta_L$ , for fixed  $\beta_S$ . This corresponds to a vertical cut of the phase diagram in panel a). The dominance of the smaller type at low  $\beta_L$ , co-existence at intermediate values, and dominance of the larger disks at high  $\beta_L$  are clearly visible.

Coexistence of both species occurs in a very limited region of the diagram, around a small area near a specific line in the  $(\beta_S, \beta_L)$  plane. An approximate characterisation of this coexistence curve can be obtained from a simple description of the dynamics in terms of rate equations. To construct these equations with proper parameters, we first consider only one type of disk in isolation, neglect fluctuations and any notion of space. We use a Lotka–Volterra model to describe the combination of death events and growth limited by volume exclusion [43],

$$\frac{dN}{dt} = -\delta N + \hat{\beta} N \left( 1 - \frac{N}{N_{\max}} \right), \quad (4)$$

where the term in the brackets ensures that the growth dynamics stops as  $N$  reaches  $N_{\max}$ ;  $\delta$  is the death rate, and  $\hat{\beta}$  is an effective growth rate.

This effective growth rate is a fitting parameter introduced in this very simple description to take into account



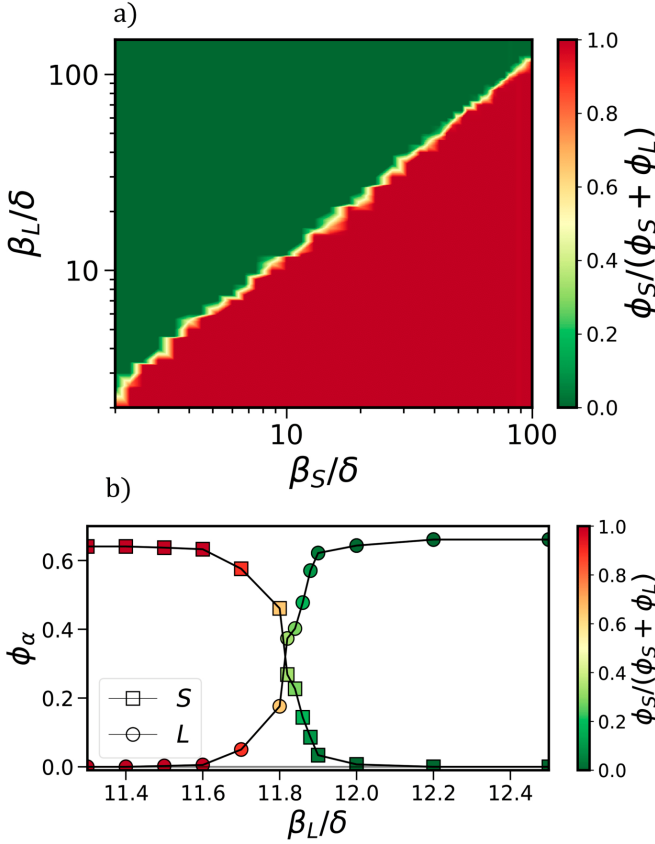


Figure 2. Coexistence diagram for the system of passive particles in the plane spanned by the birth rates  $\beta_S$  and  $\beta_L$ . Panel a): color indicates where in parameter space either type of particle dominates, or if there is co-existence. Panel b): Vertical cut in the phase diagram in (a) for  $\beta_S/\delta = 10$  showing the packing fractions for both types of disks. The colors of the symbols represent the fraction of small particles in the system.  $\delta = 0.01$ ,  $\sigma_S = 1.0$ , and  $\sigma_L = 1.2$ .

that the actual birth rate is limited by the available space, and therefore not equal to the raw birth rate  $\beta$ . We take  $\hat{\beta} = a\beta$ , where  $a$  is an unknown adimensional coefficient. In [11] we observed that the steady number of disks in a single-species model depends in a non-trivial way on the birth and death rates, the size of the particles, and on the diffusion coefficient. Thus, in this description we use  $a > 0$  and  $N_{\max}$  as fitting parameters.

We rewrite Eq. (4) in the standard form

$$dN/dt = rN(1 - N/K), \quad (5)$$

with  $r = a\beta - \delta$ . The carrying capacity  $K = N_{\max}(1 - \frac{\delta}{a\beta})$  is the effective long-time number of disks in the system.

To verify the validity of the logistic-growth approach we have carried out simulations of the model in which all particles have the same size, using a small diffusion coefficient,  $D = 0.001$ . In the long-time we compute the packing fraction  $\phi_\infty = N(t \rightarrow \infty)\pi(\sigma/2)^2/L_s^2$ . We do this for several different disk sizes ( $\sigma = 1.0, 1.2, 1.4$ ) and for some

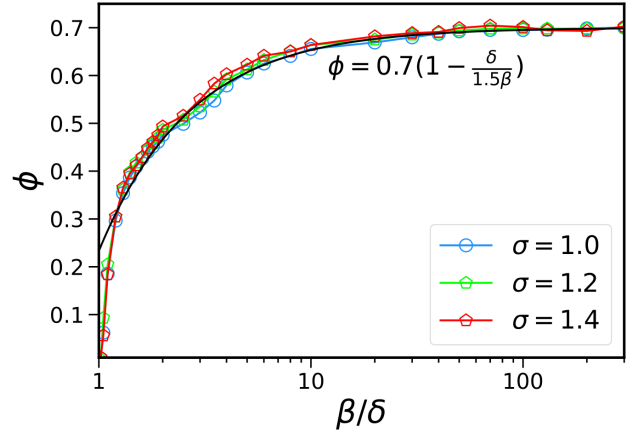


Figure 3. Long-time average packing fraction,  $\phi_\infty$ , for a system of only one type of disks as a function of the rate  $\beta$  and  $\delta = 0.01$ . The plots correspond to different disk sizes  $\sigma$  as the symbols indicate. The black line corresponds to the best fitted curve for  $a = 1.5$ , and  $\phi_{\max} = 0.7$ .

values of  $\beta$  to check the relationship  $\phi_{\text{stat}} = K\pi(\sigma/2)^2/L_s^2 = N_{\max}\pi(\sigma/2)^2/L_s^2(1 - \frac{\delta}{a\beta})$  (the stationary packing fraction of the Lotka–Volterra equation). The results are shown in Fig. 3. There is a good collapse of all the plots for the different values of  $\sigma$ , and the best fit to the expression of  $\phi_\infty$  is obtained for  $\phi_{\max} = N_{\max}\pi(\sigma/2)^2/L_s^2 = 0.7$ ,  $a = 1.5$ . This confirms that the logistic description with suitable effective parameters can be used to describe the stationary state with a single type of particle.

The Lotka–Volterra model can be generalised to the case of a binary mixture of disks. This approximate description can be useful to study the influence of one type of disks on the other, in particular, attending to their different sizes and growth rates. We assume the following Lotka–Volterra competition dynamics between the two species (which we label again  $S$  and  $L$  for ‘small’ and ‘large’ disks, respectively) [44]:

$$\begin{aligned} \frac{dN_L}{dt} &= -\delta N_L + a\beta_L \left(1 - \frac{N_L + \alpha_L N_S}{N_{L,\max}}\right) N_L, \\ \frac{dN_S}{dt} &= -\delta N_S + a\beta_S \left(1 - \frac{N_S + \alpha_S N_L}{N_{S,\max}}\right) N_S. \end{aligned} \quad (6)$$

The term  $\alpha_L N_S$  ( $\alpha_S N_L$ ) is the decline of the growth rate of  $N_L$  ( $N_S$ ) due to the presence of the smaller (larger) disks. The quantities  $N_{S,\max}$  and  $N_{L,\max}$  are the number of particles for either species at which no further growth can occur.

The dependence of the interaction terms on the ratio of disk sizes becomes more apparent if we write this equation

in terms of packing fractions:

$$\begin{aligned} \frac{d\phi_L}{dt} &= -\delta\phi_L + a\beta_L \left( 1 - \frac{\phi_L + \alpha_L \frac{\sigma_L^2}{\sigma_S^2} \phi_S}{\phi_{L,\max}} \right) \phi_L, \\ \frac{d\phi_S}{dt} &= -\delta\phi_S + a\beta_S \left( 1 - \frac{\phi_S + \alpha_S \frac{\sigma_S^2}{\sigma_L^2} \phi_L}{\phi_{S,\max}} \right) \phi_S. \end{aligned} \quad (7)$$

Now  $\phi_{\alpha,\max} = N_{\alpha,\max}\pi(\sigma_\alpha/2)^2/L_s^2$  ( $\alpha = L, S$ ). We assume that  $\alpha_L$  and  $\alpha_S$  depend on the demographic parameters of the system ( $\beta_L, \beta_S$ ), and as detailed in Appendix A. Fitting to simulation data we find

$$\begin{aligned} \alpha_L &\approx \left( \frac{\beta_S}{\beta_L} \right)^{1/4}, \\ \alpha_S &\approx \left( \frac{\beta_L}{\beta_S} \right)^{1/4}. \end{aligned} \quad (8)$$

These relations characterise the tradeoff between geometry and demography (reproduction) in the competition dynamics. For example the coefficient in the growth rate for the larger disks  $\alpha_L \frac{\sigma_L^2}{\sigma_S^2} = \frac{\sigma_L^2}{\sigma_S^2} \left( \frac{\beta_S}{\beta_L} \right)^{1/4}$  increases proportionally to  $(\sigma_L/\sigma_S)^2$ , while its dependence on the relative birth rates is much weaker and only scales as  $(\beta_S/\beta_L)^{1/4}$ .

## 2. The role of diffusion

In this subsection we study the case in which both types of passive disks have the same birth and death rates but where their diffusion coefficients are different. In biological applications situations of this type have given rise to contradictory results (albeit under very different settings) so that diffusing faster provides a competitive advantage [31] or can be detrimental [32]). Thus, one of the main questions we address is if high or low diffusivity can provide a selective advantage for either of the two competing populations. In our model diffusivity introduces a spatial scale increasing the effective size of the disks, and hence affecting the dynamics of space-limited growth.

In the upper row of Fig. 4 we show the spatial distribution of disks at long times, for different  $D_L$  and leaving all other model parameters fixed. In the leftmost panel (small ratio  $D_L/D_S$ ) the smaller particles dominate the system. In the central panel (intermediate  $D_L/D_S$ ), there is a balance of both types of disks, and when  $D_L/D_S$  is sufficiently high (rightmost panel), the larger disks occupy most of the space. Figs. 4 d)-f) show the time evolution of the packing fractions of both types in simulations starting with 250 particles of each size. The corresponding phase diagram, for  $\sigma_L/\sigma_S = 1.2$ , is shown in Fig. 5a). Increasing the diffusivity of either species promotes an increased relative abundance of that species. This is because larger diffusivity for a given particle means it effectively occupies more space

where others cannot place their offspring. In particular we observe a transition between phases in which the system is predominantly filled by the smaller particles to one in which it is mostly filled by larger particles.

We conclude that increasing diffusivity of the larger disks can reverse the competitive advantage of the smaller ones. At difference with the results of the previous subsection (Fig. 1), the dominance of larger disks for high  $D_L/D_S$  is not complete though. Instead, we find a remaining population of smaller disks occupying about 10-15% of space until the end of our simulations (i.e.,  $\phi_S = 0.1-0.15$ ), see Fig. 5b). We attribute this to interstitial holes, i.e., empty space between the disks, noting that the effect is more pronounced (i.e.,  $\phi_S/(\phi_S + \phi_L)$  becomes larger) when the ratio  $\sigma_L/\sigma_S$  is increased (see Fig. 6).

An exception to the survival of the smaller disks can be observed in a region in  $(D_S, D_L)$  space in which the larger disks almost completely dominate the system [dark green to the lower left in Fig. 5a)]. This dominance only occurs when  $D_S$  is small enough so that the movement of the smaller disks is negligible with respect to their lifetime. This region disappears as the ratio  $\sigma_L/\sigma_S$  becomes larger (see Fig. 6), so that we think it is because small disks may occupy the interstitial holes.

## B. Active particles

We consider systems in which both types of disks are self-propelled, possibly with different values of the propulsion velocities  $v_L$  and  $v_S$ . The remaining parameters are set to the same:  $\beta_L = \beta_S = \beta$ ,  $D_L = D_S = D$ , and  $\delta = 0.01$ .

We first take a birth rate of  $\beta = 0.05$ , and diffusivity of  $D = 0.05$ . Under these conditions, without activity, the system is in a liquid state, which means that the packing fraction of both types is low and there is no ordering. Also the system reaches the steady state faster. Our motivation for this choice is that we aim at analysing MIPS, which is typically not observed for large values of the packing fraction (solid phase) [11, 15].

In the previous section we have shown that Brownian mobility provides an advantage in the competition for space between the two types of disks. Given that self-propulsion yields comparable effects (at low velocities) to diffusivity [45, 46] we expect in this low activity regime similar outcomes for active particles. However, MIPS typically appears when activity is large, and thus we study this regime in detail by varying the self-propulsion coefficients of both types of disks, and compute the average packing fraction of each species at long times.

The resulting phase diagram, obtained for  $\sigma_L/\sigma_S = 1.2$ , is shown in Fig. 7a). When the activity of both types of disks is sufficiently low the smaller disks dominate the system. As  $v_L$  increases (keeping  $v_S$  fixed at a sufficiently small value) a transition to coexistence is found. This coexistence remains

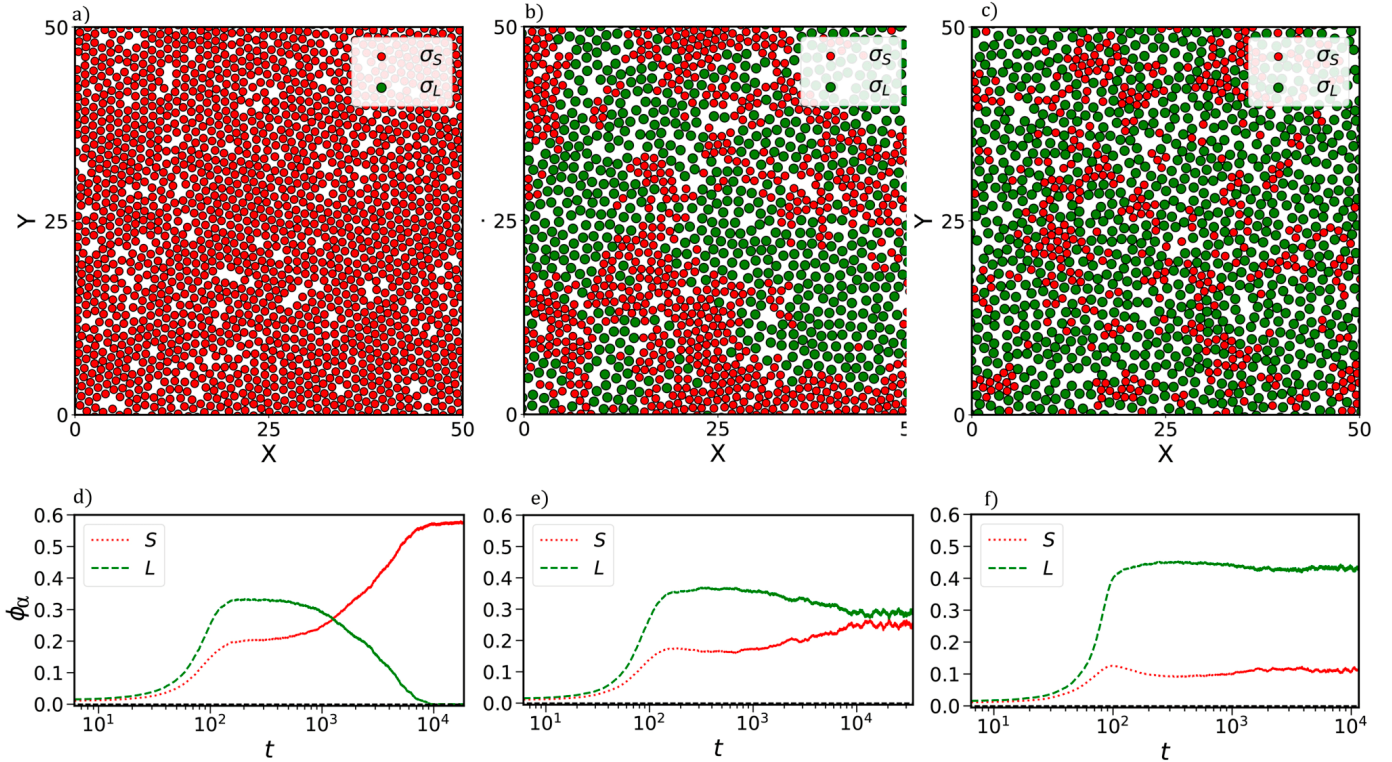


Figure 4. Panels in the first row [a]-d)] show snapshots of the spatial distribution of passive disks space at long times (graphs only show a part of the full system, which has lateral size  $L_s = 150$ ). Panels in the second row [e]-h)] show the corresponding time evolution of the packing fractions for both species, starting with a random configuration of 250 disks of each type. In the different columns we have used different values of  $D_L$  and  $D_S = 0.001$ :  $D_L = 0.01, 0.02, 1.0$  from left to right. Remaining parameters are  $\delta = 0.01$ ,  $\beta = 0.05$ ,  $\sigma_L/\sigma_S = 1.2$ .

as the activity of the larger particles is further increased. We find interesting behaviour for sufficiently large  $v_S$ . This is the region of MIPS. We observe that coexistence can be reached for low and intermediate values of  $v_L$  (see Fig. Fig. 7 b)). In between there is a range of values where large particles dominate, and for very high  $v_L$  small particles dominate the system.

Which type of particle survives (or the presence of coexistence) results from a complicated interplay between the separation in dense and diluted phases formed of both species in non-steady conditions because of activity, and the birth/death dynamics which is itself mediated by the spatial distribution of disks. This is shown in the upper panels of Fig. 8 with some examples of the disk distribution at long times for  $v_S = 50$ , and different values of  $v_L$ . In panel a) there is coexistence for sufficiently small  $v_L$ . As we increase  $v_L$  the smaller species becomes extinct (dark green region in the phase diagram) [Fig. 7b)]. As  $v_L$  is increased further, coexistence is observed again and both species show MIPS [see Fig. 8c)]. For even higher values of  $v_L$ , the large disks become extinct [see Fig. 8d)]. In the lower row we show the corresponding time evolutions of the packing fractions of both types of particles starting from a configuration with 250 particles of each.

Let us next characterise the emerging spatial structures when there is coexistence. To do this we compute the distribution of local packing fractions of large disks,  $P(\phi_L)$ , and small ones,  $P(\phi_S)$ . These are obtained from the local packing fraction of either species at each location in space. MIPS is characterised by a double-peaked distribution, with the two peaks corresponding to the dense and diluted phases, respectively [15]. In Fig. 9a) we plot  $P(\phi_S)$  and  $P(\phi_L)$  corresponding to two situations: i) small particles with very low  $v_S = 0.1$ , and large particles with low  $v_L = 10$  (the two distributions are plotted in red); ii) small particles again with  $v_S = 0.1$ , but large particles with high  $v_L = 150$ . These scenarios correspond, respectively, to the cases where (if the two types were in isolation without the presence of the other) a) neither small nor large disks would form MIPS, and b) small disks would not form MIPS, but large ones would because they have a high  $v_L$ . However when both types of particles are present in the system, the distribution of local packing fractions is single-peaked, and there is no separation between dilute and dense phases.

Instead, in Fig. 9b) we use a higher value of  $v_S = 50$ , and two different values of  $v_L$ :  $v_L = 25$  for which there would be no MIPS for the large particles in isolation, and  $v_L = 56$ , for which there would be MIPS. Now  $P(\phi_L)$  and  $P(\phi_S)$  are double-peaked, that is both types of disks have a dense and



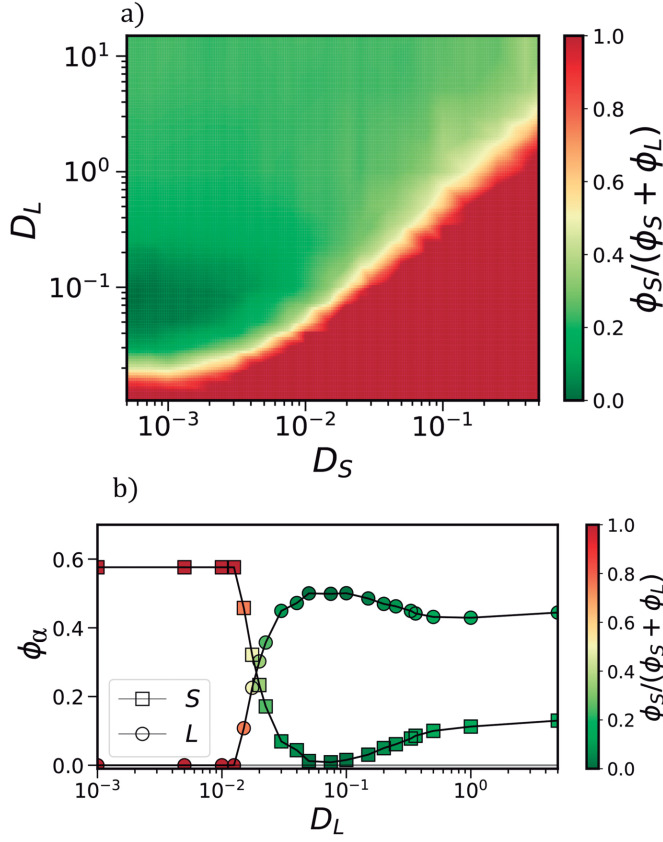


Figure 5. Phase diagram in the space of diffusivities,  $D_S$  and  $D_L$ . Panel a): Background color indicates the relative filling fraction of the two type of disks. In the red region the smaller particles fill most of the space, in the green region the larger particles dominate. Panel b): Long-time average packing fractions for both species as a function of  $D_L$ , for fixed  $D_S = 0.001$ . The colors of the symbols indicate the relative amount of space occupied by the small particles. Model parameters are  $\delta = 0.01$ ,  $\beta_L = \beta_S = 0.05$ ,  $\sigma_S = 1.0$ ,  $\sigma_L = 1.2$ .

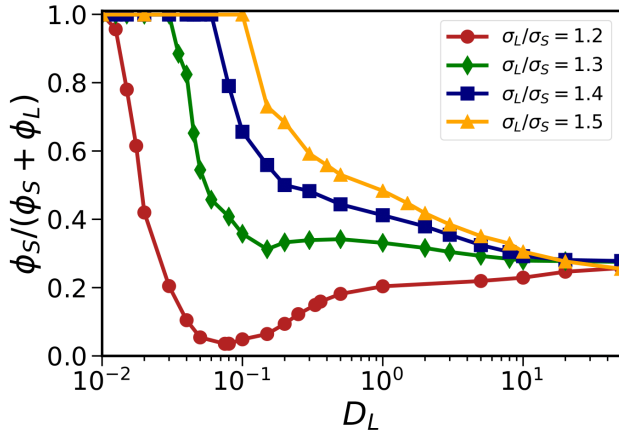


Figure 6. Normalized packing fraction of small particles versus  $D_L$  for different values of  $\sigma_L/\sigma_S$  as indicated. Same remaining parameters as in Fig. 5

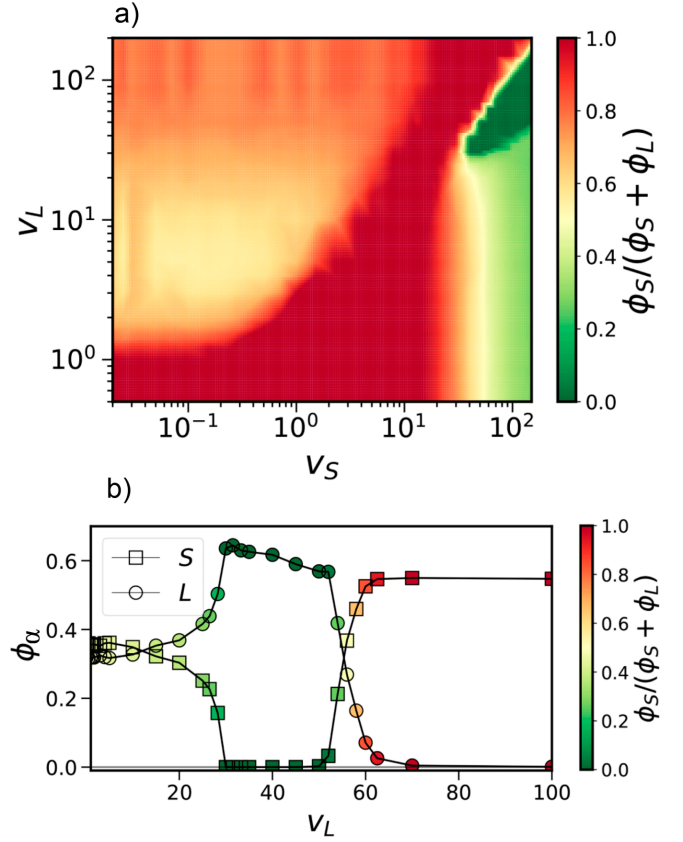


Figure 7. Panel (a): Phase diagram of the system with active disks in the  $(v_L, v_S)$  plane. Background color represents the normalised packing fraction of the smaller particles (darker red color indicates dominance of the smaller type, darker green dominance of the larger). Panel (b): Long-time average packing fractions for both species as function of  $v_L$  for fixed  $v_S = 50$ . The colors of the symbols indicate the relative space occupied by the small particles. Model parameters are  $\delta = 0.01$ ,  $\beta_L = \beta_S = 0.05$ ,  $\sigma_S = 1.0$ ,  $\sigma_L = 1.2$ .

a dilute phase. These results indicate that the two species arrange in the same spatial distribution when they coexist. Either both display a single phase, or both species show MIPS.

Finally, in Fig. 10 we plot the normalized packing fraction for the smaller types of disks when  $v_L$  varies (keeping  $v_S = 50$  fixed, i.e., within the MIPS region) and for several values of the ratio of size particles. When we increase  $\sigma_L/\sigma_S$ , the effect of the interstices becomes more pronounced which causes the small particles packing fraction to increase. For the same reason the region in Fig. 10 in which the smaller particles go extinct reduces. In other words, as  $\sigma_L/\sigma_S$  increases, the large particles need a higher value of activity to form MIPS. This results in a higher value of  $v_L$  for the small particles to go extinct.

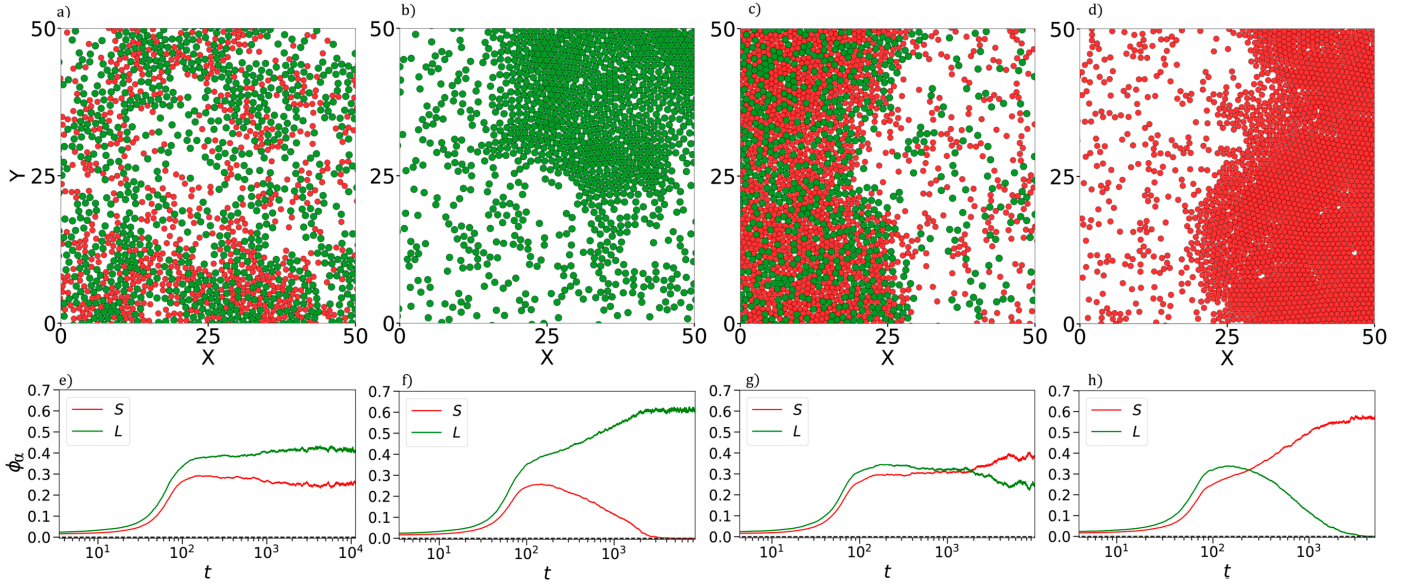


Figure 8. Panels in the first row (a-d) show snapshots of the spatial distribution of active disks space at long times (only a part of the full size  $L_s = 150$ ). Panels in the second row (e-h) correspond to the temporal evolution of the packing fraction starting with a random configuration of  $250 + 250$  disks. In addition, for each column, we have used different values of  $v_L$  and  $v_S = 50$ . The values used are  $v_L = 25, 40, 56$  and  $70$  from left to right.

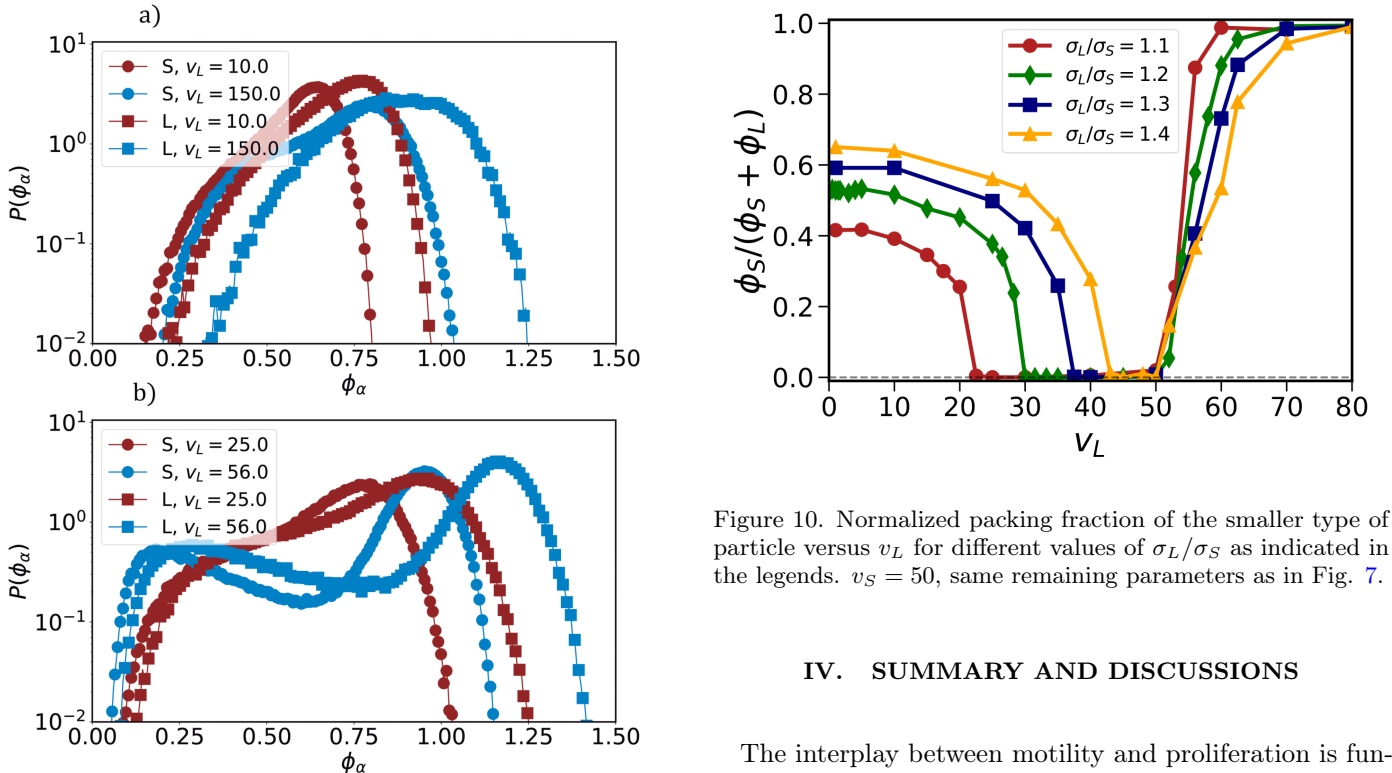


Figure 9. Distribution of the local packing fraction for different values of activity in configurations where both disks types coexist. Panel (a):  $v_S = 0.1$ . Panel (b):  $v_S = 50$ . The  $v_L$  value is shown in the legend.

Figure 10. Normalized packing fraction of the smaller type of particle versus  $v_L$  for different values of  $\sigma_L/\sigma_S$  as indicated in the legends.  $v_S = 50$ , same remaining parameters as in Fig. 7.

#### IV. SUMMARY AND DISCUSSIONS

The interplay between motility and proliferation is fundamental for many biological processes. In this work we have studied a binary mixture of two types of motile disks with different sizes, and undergoing birth and death dynamics. At difference with our previous work [11] where we concentrated on the spatial structure formed by a single population of identical disks, in this work we have studied the conditions for coexistence and which of the two types does not go extinct in the long-time. Since the birth proba-



bility is limited by size, smaller disks have larger chances to reproduce (when the remaining characteristics are identical). Thus we focused on the conditions under which this is reversed, i.e., larger disks survive, or there is coexistence of both types of disks. We have considered two main cases: passive and self-propelled disks. For passive particles we have discussed the role of growth rates and diffusivities, and have obtained typical phase diagrams when the ratio of particles sizes is  $\sigma_L/\sigma_s = 1.2$ , but discussed also it for other ratios, unveiling the role of interstices. We observe that Brownian mobility provides with an advantage such that the larger particles, with less chances to reproduce, can coexist with the smaller or even dominate in the steady state when they diffuse faster.

We have analysed the role of activity and have shown that, as expected, it is similar similar to that of diffusivity when self-propelled velocities have low values. However, when MIPS is present (typically obtained for larger values of activities) the coexistence dynamics changes, and the typical situation is a coexistence of both species, and both showing the same diluted and dense phases.

Further work should be devoted to analyse the spatial structure in the different situations we have described, and in particular, the influence on the hexatic and solid phases, if any, of the binary mixture with demography. Concerning biological applications, the main motivation for our work, where populations are characterized by large diversity, it is of great interest to consider not only two disks sizes but a whole size distribution, but also of the other parameters like the growth rates and the self-propulsion velocities.

## ACKNOWLEDGMENTS

A.A and C.L. acknowledge grant LAMARCA PID2021-123352OB-C32 funded by MCIN/AEI/10.13039/501100011033323 and FEDER “Una manera de hacer Europa”. T.G. acknowledges partial financial support from the Agencia Estatal de Investigación and Fondo Europeo de Desarrollo Regional (FEDER, UE) under project APASOS (PID2021-122256NB-C21, PID2021-122256NB-C22), and the Maria de Maeztu programme for Units of Excellence, CEX2021-001164-M funded by MCIN/AEI/10.13039/501100011033.

## Appendix A

The parameters for which both species coexist can be approximated from the non-zero fixed points of Eqs. (7):

$$\begin{aligned}\phi_S^* &= \kappa_S - \alpha_S \phi_L^* \left(\frac{\sigma_S}{\sigma_L}\right)^2, \\ \phi_S^* &= \frac{1}{\alpha_L} (\kappa_L - \phi_L^*) \left(\frac{\sigma_S}{\sigma_L}\right)^2,\end{aligned}\quad (\text{A1})$$

with

$$\begin{aligned}\kappa_S &= \frac{a\beta_S - \delta}{a\beta_S} \phi_{S,\max}, \\ \kappa_L &= \frac{a\beta_L - \delta}{a\beta_L} \phi_{L,\max}.\end{aligned}\quad (\text{A2})$$

Both equalities are fulfilled at the same time in the coexistence region. Furthermore, recall that  $\phi_{S,\max} = \phi_{L,\max}$ , since the maximum value does not depend on either the type of particle or the size of the system. Now, we make the ansatz:

$$\begin{aligned}\alpha_S &= c_S (\beta_L/\beta_S)^\gamma, \\ \alpha_L &= c_L (\beta_S/\beta_L)^\gamma,\end{aligned}\quad (\text{A3})$$

where  $c_S$ ,  $c_L$  and  $\gamma$  are constants.

We have assumed symmetry in the interaction of the species, so that both species have the same exponent  $\gamma$ . Inserting the ansatz (A3) in Eq. (A1) we obtain an expression for the packing fraction with explicit dependence on the demographic rates:

$$\begin{aligned}\phi_S^* &= \frac{1}{1 - c_L c_S} \left( \kappa_S - \kappa_L c_S \left(\frac{\beta_L}{\beta_S}\right)^\gamma \left(\frac{\sigma_S}{\sigma_L}\right)^2 \right), \\ \phi_L^* &= \frac{1}{1 - c_L c_S} \left( \kappa_L - \kappa_S c_L \left(\frac{\beta_S}{\beta_L}\right)^\gamma \left(\frac{\sigma_L}{\sigma_S}\right)^2 \right).\end{aligned}\quad (\text{A4})$$

These expressions predict the value of the steady packing fractions at each point of the diagram  $(\beta_L, \beta_S)$  inside the coexistence region. In the region where only large (small) particles are found, we have  $\phi_L^* = \kappa_L$  and  $\phi_S^* = 0$  ( $\phi_L^* = 0$  and  $\phi_S^* = \kappa_S$ ).

We have carried out a series of numerical experiments for various values of  $\delta$ ,  $\sigma_L$ ,  $\sigma_S$ , (not shown) beyond those used in Fig. 2 and have observed that the phase diagram is almost independent of the value of  $\delta$  (always assuming  $\beta > \delta$ ), and the ratio  $\sigma_L/\sigma_S$ . The coefficients  $c_L$ ,  $c_S$  and  $\gamma$  in Eq. (A4) can be obtained from fits of the packing fraction (see Fig. 11). We compute the difference between the packing fraction obtained from Eq. (A4), and the one obtained from the numerical simulations of the particle model for different values of  $\delta$ ,  $\sigma_S$ ,  $\sigma_L$ ,  $\beta_S$ ,  $\beta_L$ . Then, we minimize the sum of all the differences.

From these simulations, the best fit is obtained for  $c_L = 0.69$ ,  $c_S = 1.34$  and  $\gamma = 1/8$ .

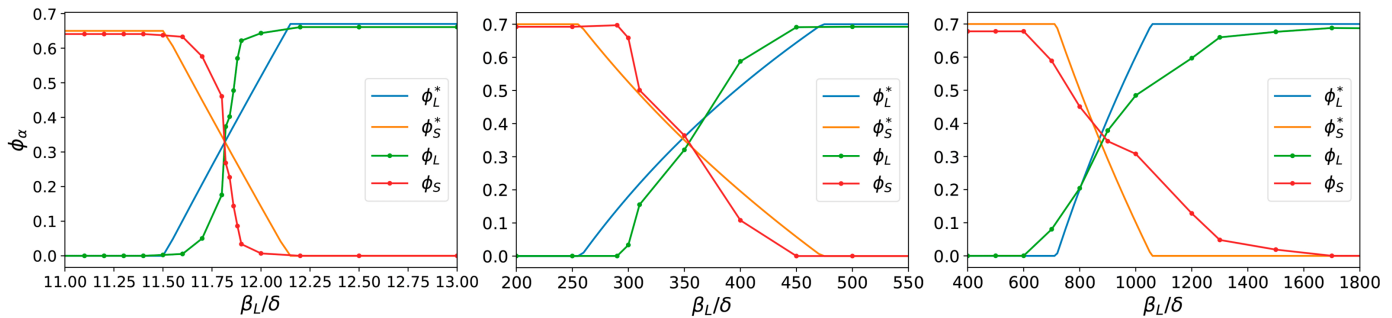


Figure 11. Long-time average packing fractions for both species as a function of  $\beta_L/\delta$ , for fixed  $\beta_S = 0.1$  (left) and  $\beta_S = 0.85$  (middle and right), and  $\delta = 0.01$ .  $\phi_\alpha^*$  obtained from Eq. (A4) and  $\phi_\alpha$  from particle simulations. From left to right:  $\sigma_L/\sigma_S = 1.2, 1.3, 1.4$ .

- 
- [1] R. Alert and X. Trepat, *Annual Review of Condensed Matter Physics* **11**, 77 (2020).
- [2] R. Alert and X. Trepat, *Physics Today* **74**, 30 (2021).
- [3] N. Sepúlveda, L. Petitjean, O. Cochet, E. Grasland-Mongrain, P. Silberzan, and V. Hakim, *PLOS Computational Biology* **9**, 1 (2013).
- [4] T. E. Angelini, E. Hannezo, X. Trepat, M. Marquez, J. J. Fredberg, and D. A. Weitz, *Proceedings of the National Academy of Sciences* **108**, 4714 (2011).
- [5] C. A. M. La Porta and S. Zapperi, *The Physics of Cancer* (Cambridge University Press, 2017).
- [6] B. Szabó, G. J. Szöllösi, B. Gönci, Z. Jurányi, D. Selmeczi, and T. Vicsek, *Phys. Rev. E* **74**, 061908 (2006).
- [7] O. Hallatschek, S. S. Datta, K. Drescher, J. Dunkel, J. Elgeti, B. Waclaw, and N. S. Wingreen, *Nature Reviews Physics* **5**, 407 (2023).
- [8] Y. Tang, S. Chen, M. Bowick, and D. Bi, (2023), [10.48550/arXiv.2303.00129](https://arxiv.org/abs/2303.00129).
- [9] Y. Kim, S. Joo, W. K. Kim, and J.-H. Jeon, *Macromolecules* **55**, 7136 (2022).
- [10] Y. Du, H. Jiang, and Z. Hou, *Soft Matter* **15** (2019), [10.1039/C8SM02292E](https://doi.org/10.1039/C8SM02292E).
- [11] A. Almodóvar, T. Galla, and C. López, *Phys. Rev. E* **106**, 054130 (2022).
- [12] P. Romanczuk, M. Bär, W. Ebeling, B. Lindner, and L. Schimansky-Geier, *The European Physical Journal Special Topics* **202**, 1 (2012).
- [13] B. ten Hagen, S. van Teeffelen, and H. Löwen, *Journal of Physics: Condensed Matter* **23**, 194119 (2011).
- [14] Y. Fily and M. C. Marchetti, *Phys. Rev. Lett.* **108**, 235702 (2012).
- [15] P. Digregorio, D. Levis, A. Suma, L. F. Cugliandolo, G. Gonnella, and I. Pagonabarraga, *Phys. Rev. Lett.* **121**, 098003 (2018).
- [16] L. Caprini, U. M. B. Marconi, C. Maggi, M. Paoluzzi, and A. Puglisi, *Phys. Rev. Research* **2**, 023321 (2020).
- [17] E. P. Bernard and W. Krauth, *Phys. Rev. Lett.* **107**, 155704 (2011).
- [18] J. U. Klamser, S. C. Kapfer, and W. Krauth, *Nature Communications* **9**, 5045 (2018).
- [19] F. F. Abraham, *Physics Reports* **80**, 340 (1981).
- [20] D. R. Nelson and B. I. Halperin, *Phys. Rev. B* **19**, 2457 (1979).
- [21] M. E. Cates and J. Tailleur, *Annual Review of Condensed Matter Physics* **6**, 219 (2015).
- [22] I. Buttinoni, J. Bialké, F. Kümmel, H. Löwen, C. Bechinger, and T. Speck, *Phys. Rev. Lett.* **110**, 238301 (2013).
- [23] T. Biben and J.-P. Hansen, *Phys. Rev. Lett.* **66**, 2215 (1991).
- [24] D. Frenkel and A. A. Louis, *Phys. Rev. Lett.* **68**, 3363 (1992).
- [25] J. Russo and N. B. Wilding, *Phys. Rev. Lett.* **119**, 115702 (2017).
- [26] G. Larwood and B. Rosen, *Biology and Systematics of Colonial Organisms*, Physiological Ecology (Systematics Association, 1979).
- [27] J. B. C. Jackson, *The American Naturalist* **111**, 743 (1977).
- [28] L. M. Ponczek and N. W. Blackstone, *The Biological Bulletin* **201**, 76 (2001), PMID: 11526066.
- [29] S. Das, S. Ghosh, and R. Chelakkot, *Phys. Rev. E* **102**, 032619 (2020).
- [30] A. Reversat, F. Gaertner, J. Merrin, J. Stopp, S. Tasciyan, J. Aguilera, I. de Vries, R. Hauschild, M. Hons, M. Piel, A. Callan-Jones, R. Voituriez, and M. Sixt, *Nature* **582**, 582 (2020).
- [31] S. Pigolotti and R. Benzi, *Phys. Rev. Lett.* **112**, 188102 (2014).
- [32] E. Heinsalu, E. Hernández-García, and C. Lopez, *Physical review. E, Statistical, nonlinear, and soft matter physics* **85**, 041105 (2012).
- [33] M. C. Marchetti, J. F. Joanny, S. Ramaswamy, T. B. Liverpool, J. Prost, M. Rao, and R. A. Simha, *Rev. Mod. Phys.* **85**, 1143 (2013).
- [34] C. Bechinger, R. Di Leonardo, H. Löwen, C. Reichhardt, G. Volpe, and G. Volpe, *Rev. Mod. Phys.* **88**, 045006 (2016).
- [35] V. Hakim and P. Silberzan, *Reports on Progress in Physics* **80**, 076601 (2017).
- [36] I. Grobas, M. Polin, and M. Asally, *eLife* **10**, e62632 (2021).
- [37] P. K. Bommineni, N. R. Varela-Rosales, M. Klement, and M. Engel, *Phys. Rev. Lett.* **122**, 128005 (2019).
- [38] P. Sampedro Ruiz, Q.-l. Lei, and R. Ni, *Communications Physics* **2**, 70 (2019).
- [39] P. Sampedro Ruiz and R. Ni, *The Journal of Chemical Physics* **153**, 174501 (2020).
- [40] S. Kumar, J. P. Singh, D. Giri, and S. Mishra, *Phys. Rev. E* **104**, 024601 (2021).
- [41] H. A. Lorentz, *Annalen der Physik* **248**, 127 (1881).
- [42] C. L. Brooks, *Journal of Solution Chemistry* **18**, 99 (1989).
- [43] N. Khalil, C. López, and E. Hernández-García, *Journal of Statistical Mechanics: Theory and Experiment* **2017**,

- 063505 (2017).
- [44] L. Edelstein-Keshet, [Mathematical Models in Biology](#) (Society for Industrial and Applied Mathematics, 2005).
- [45] D. Levis and L. Berthier, [EPL \(Europhysics Letters\)](#) **111** (2015), 10.1209/0295-5075/111/60006.
- [46] J. Palacci, C. Cottin-Bizonne, C. Ybert, and L. Bocquet, [Phys. Rev. Lett.](#) **105**, 088304 (2010).